Acceptance and usability of a soft robotic, haptic feedback seat for autonomy level transitions in highly automated vehicles

Jan Peters, *Student Member, IEEE*, Bani Anvari, Johann Licher, Mats Wiese, *Student Member, IEEE*, Annika Raatz, *Member, IEEE*, Helge A. Wurdemann, *Member, IEEE*

***Abstract*—Fully autonomous vehicles, capable of completing entire end-to-end journeys without the interference of a human driver, will be one of the biggest transforming technologies of the next decades. As the journey towards fully autonomous vehicles progresses, there will be an increase in the number of highly automated vehicles on the roads, requiring the human driver to take back control in situations, which cannot be handled by the vehicle autonomously. These human-robot take-over requests can lead to safety risks, in particular in scenarios when the driver fails to understand the take-over request and, hence, lacks situational awareness. This paper presents the acceptance and usability assessment of a haptic feedback driver seat capable of informing the driver of a take-over request through static mechano-tactile haptic feedback. The seat is equipped with an embedded array of soft pneumatic actuators, that have been fully modelled and characterised. The evaluation process of the haptic feedback seat engaged 21 participants who experienced both auditory and haptic feedback from the seat in a number of simulation experiments within a driving simulator. The vehicular technology was assessed through well-established methods to understand the acceptance (usefulness and satisfaction) and usability of the haptic feedback driver seat.**

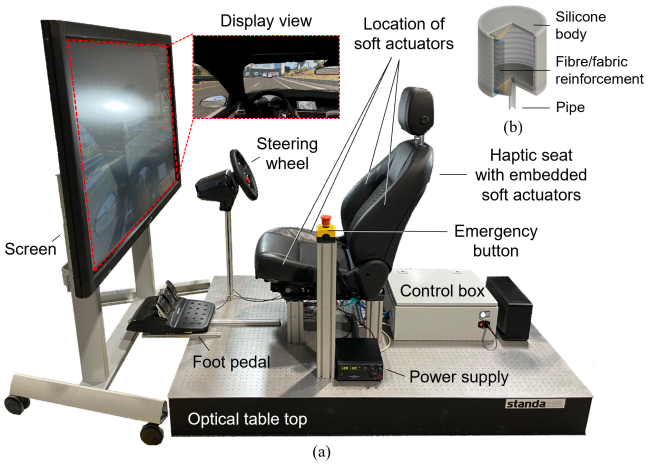

Fig. 1. (a) The haptic feedback seat, its control box, and power supply are in front of a 65-inch screen on a Honeycomb optical table top. A steering wheel and foot pedal complete the driving simulator setup. 12 soft actuators are embedded into the bottom and back side bolsters of the seat. (b) The actuator is made of a silicone material, reinforced using fibres and fabric meshes.

I. Introduction

With the paradigm shift towards driverless, fully autonomous vehicles, the uptake of highly automated cars will significantly increase [1]. Highly automated vehicles are characterised by different levels of autonomy supported by assistive technologies. The Society of Automotive Engineers has introduced six levels of driving automation ranging from 0 (fully manual) to 5 (driverless/fully autonomous) depending on the autonomy features of the Advanced Driving Assistance System (ADAS) provided to drivers [2]. In autonomy levels 1 and 2, the vehicle possesses some capability to perform specific tasks such as (adaptive) cruise control or lane changing; however, the driver must maintain constant awareness of their surroundings and be prepared to intervene when needed as the liability of any incident is with the human driver. Starting from level 3 the driver can be engaged in tasks other than driving, commonly referred to as secondary tasks. The liability is now with the vehicle manufacturer. In level 3, the vehicle is able to handle some driving tasks under certain circumstances, specifically within a well-defined environment (e.g., driving on a highway with a centre strip). During these situations, the driver is allowed to engage in secondary tasks, however, the driver is required to intervene within a short time if the system requires them to do so. In level 4, the vehicle can also drive autonomously under certain situations and return to a state of minimal risk, e.g., safely stopping on the hard shoulder, if the driver does not react to a take-over request. Level 5 describes full driving automation. No driver is required as the car can handle all driving functions at all times. The passengers in a vehicle providing level 5 only need to provide navigational input [3]. By 2035, it is predicted that vehicles with autonomy levels 3-5 will reach 58% of total sales [1].

During the transition from higher to lower levels of autonomy, the driver must actively engage both cognitively and physically. They need to maintain full awareness of the surrounding environment, monitor the vehicle, and be prepared to take control in a timely and intuitive manner when the vehicle's ADAS is unable to handle the situation effectively [4], [5]. To notify the driver of an impending unresolved situation,

*This work is supported by the Engineering and Physical Sciences Research Council (grant numbers: EP/R037795/1 and EP/S014039/1) and UKRI Trustworthy Autonomous System HUB (grant number: EP/V00784X/1).

J. Peters and H.A. Wurdemann are with the Department of Mechanical Engineering, University College London, UK e-mail: h.wurdemann@ucl.ac.uk.

B. Anvari is with the Department of Civil, Environmental and Geomatic Engineering, University College London, UK e-mail: b.anvari@ucl.ac.uk.

J. Peters, J. Licher, M. Wiese, and A. Raatz are with the Institute of Assembly Technology, Leibniz University Hannover, Germany email: peters@match.uni-hannover.de.

Manuscript received XX XX, XX; revised XX XX, XX.

such as reaching programmatic limits or encountering a potentially dangerous scenario, the vehicle issues a take-over request (TOR) to prompt the driver to manually resume the driving task. In commercially available vehicles, feedback systems incorporate visual cues (e.g., displayed on the dashboard, steering wheel, middle console, or head-up display) as well as non-vocal auditory cues (e.g., audio chimes) [6]–[8].

Research has concluded that audio and visual feedback can benefit a take-over activity through the introduction of vibro-tactile cues [9], [10], [17]. Haptic feedback, in particular, becomes a viable solution for inclusive TORs for drivers with hearing impairments in highly automated vehicles. Such drivers may struggle to differentiate audio feedback from environmental sound or may have difficulty hearing the feedback altogether. Additionally, relying solely on visual cues from the dashboard may not prove feasible in such scenarios. In particular, previous studies have concentrated on providing warning or directional information, often using vibro-tactile actuators that stimulate multiple areas of the body [10]–[15], [18]. However, it has been noted that the effectiveness of high-frequency vibro-tactile feedback is limited, attributed to potential discomfort and problems such as tactile clutter [11], [15]. Understanding the advantages of high-frequency vibro-tactile feedback for urgent TORs and warning messages to the driver and its limitation for long-duration and continuous feedback, as previously reported [11], [15], our research explored the use of ambient, less-intrusive static mechano-tactile feedback [12] for less critical, non-urgent TORs, to inform and guide the driver to take back control.

This paper presents acceptance and usability results of providing static mechano-tactile haptic feedback through a haptic driver seat (see Fig. 1). Through the activation of an array of embedded soft pneumatic actuators (SPAs), the seat is capable of informing the driver of a TOR. The experiments aim at thoroughly understanding both the acceptance (encompassing usefulness and satisfaction), assessing whether potential drivers would utilise the system, and the usability, evaluating the quality of the user's interaction and ease of use of the haptic feedback driver seat. Both aspects are crucial in the success of technology. The acceptance model employs the toolkit by Van der Laan et al., which is tailored for this purpose [29]. The System Usability Scale was also utilised to understand the system's usability, as detailed by Brooke [33].

Section II provides a review of available haptic feedback technology for automated vehicles. In Section III, the soft robotic actuator used as the haptic feedback mechanism is presented in detail. For validation experiments with human participants, a driving simulator was created, described in Section IV, while the experimental setup and protocol are detailed in Section V. The results presented in Section VI are discussed in Section VII. Section VIII draws conclusions for future employments of soft robotic, haptic driver seats for autonomy level transitions in highly automated vehicles.

II. Haptic feedback driver seats: a review

A number of haptic feedback seats have been developed for vehicles aiming, e.g., to provide alerts or enhance driver comfort. In particular, researchers have focused on implementing vibro-tactile motors into seats which have been reported to enable the driver to react faster to a TOR than text-based [9] and auditory cues [17], while observing low frustration in the driver [9]. Telpaz et al. found that employing haptic feedback compared to a no-warning control group resulted in a more thorough scan of the environment in the seconds after issuing the TOR, which led to more situational awareness [18]. Although general high satisfaction levels are achieved, Chang et al. found that their vibro-tactile seat returns lower satisfaction levels than auditory systems [17]. Fitch et al. point out that giving several stimuli using haptic feedback is also suitable for directional cues, whereas overloading the driver with cues resulted in performance deterioration [19]. In 2015, General Motors (GM) launched their Safety Alert Seat using pulsing driver seat vibration to communicate potential dangers [20]. This seat works together with the automated driving support systems such as Front or Rear Parking Assist (RPA), Front Pedestrian Alert (FPA), Forward Collision Alert (FCA), and Lane Departure Warning (LDW) [20].

In recent years, several manufacturers have utilised pneumatic air cushions in seats due to their characteristics of comfort, silence, and cost-effectiveness across different industries, including the automotive and airplane industries. Switzerland-based company Lantal Textiles has developed similar pneumatic seat structures known as the Pneumatic Comfort System [21], [22]. This system replaces traditional foam cushions with inflatable seat cushions, allowing passengers to sit or lie on the seat comfortably. The air volume can be automatically adjusted by the controller to optimise passenger comfort. This type of structure, commonly used in the aerospace field, offers benefits such as light weight, adjustable stiffness, lumbar support, massage capabilities, and dynamic contouring. The seat can even be fully reclined to serve as a mattress, further enhancing the passengers' comfort experience. In the automotive industry, Volvo and Kongsberg Automotive have investigated a pneumatically actuated seat support system specifically designed for automobile applications [23], [24]. For instance, one system includes pneumatic lumbar support to provide relaxation for occupants while supporting the memory seat function, a massage system to increase driver comfort, and bolster systems to maintain the correct positioning of the customer. Continental introduced a more advanced pneumatic seat known as Seat Comfort Systems. This innovative system utilises the Pneumatic Seat Control System to optimise driving comfort [25], [26]. The seat incorporates a dynamic support function, acting as an active driver that automatically adjusts the shape of the pneumatic bag positioned near the driver's waist. This dynamic support feature enhances the overall comfort experience during driving.

Overall, existing research has shown that combining haptic feedback with audio and visual cues can have positive effects on the outcome of TORs [9], [10], [17]. When it comes to haptic feedback, it has been noted that high-frequency vibro-tactile stimulation can be attributed to potential discomfort and, e.g., tactile clutter [11], [15]. Static mechano-tactile feedback, on the other hand, might achieve attentional salience for non-urgent TORs, primarily through the actuation profile and pressure [40].

III. Design, Fabrication, and Characterisation of a Soft Pneumatic Actuator for Haptic Feedback

In Section III-A, the design and fabrication process of a single soft robotic actuator is presented. A number of these soft robots are integrated into a driver seat (see Section IV). The actuator incorporates a soft material that ensures sufficient comfort, while the use of pneumatic actuation in the reinforced chamber enables the generation of adequate force and elongation capability. In Section III-B, an in-depth explanation of an analytical modelling tool is provided that accurately predicts the actuator's output force and elongation based on the design parameters. The validity of the model is demonstrated through experiments conducted in Section III-C. By utilising this modelling tool, the actuator can be designed and fabricated to meet the desired force and elongation requirements specific to a given application.

A. Design & fabrication of the Soft Pneumatic Actuator (SPA)

The design of the soft actuator is shown in Fig. 2 (a). Multiple layers of silicone are specifically engineered to address certain challenges: To mitigate the occurrence of the radial balloon phenomenon and achieve unidirectional elongation, Ecoflex 00-30 silicone (Smooth-On) layers are reinforced with a polyester fibre (Gütermann GmbH, Knorr Prandell Mara 120). Additionally, to enhance stability against shear forces and prevent undesired radial movements, the outer wall of the chamber is lined with a two-way stretch fabric. To maintain the integrity of the actuator's upper and lower surfaces and prevent bulging during operation, an inextensible fabric (Jackson's Art, 43T Polyester Mesh) is incorporated along with an additional layer of stiffer silicone, Dragon Skin 30 silicone (Smooth-On). This combination enhances the actuator's shape stability. Air pressure is supplied to the soft actuator through a pipe inlet located at the bottom. It is important to note that the actuator design presented here builds upon and further refines the design previously described in [27].

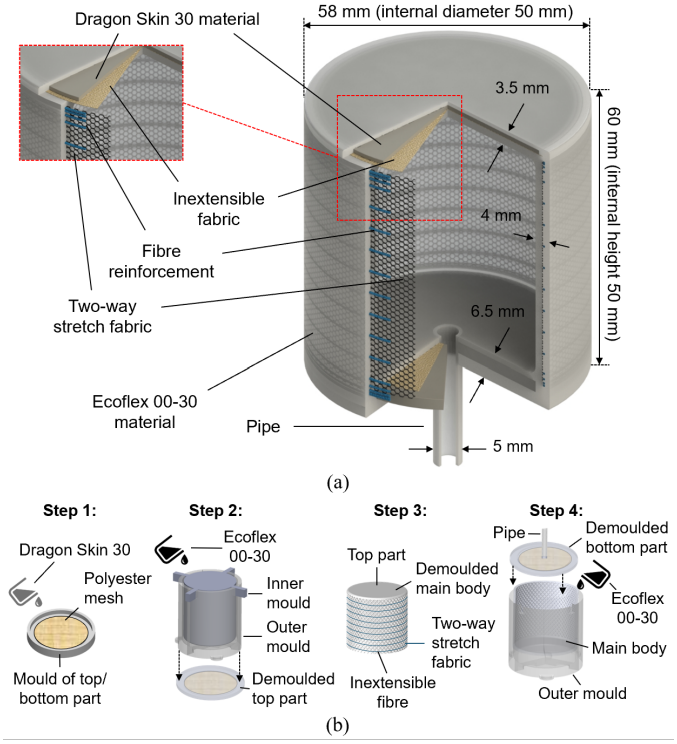

Fig. 2. (a) The cylindrically shaped actuator has a diameter of 58 mm and a height of 60 mm. The actuator comprises different reinforcements: A fibre reinforcement (blue) prevents radial expansion of the actuator while allowing elongation. The two-way stretch fabric (black) prevents buckling of the actuator when loaded axially. Ecoflex 00-30 silicone is used for the main body. Inextensible fabric (brown) embedded into Dragon Skin 30 silicone (grey) reinforces the top and bottom of the actuator. (b) Methodology for the fabrication of the soft actuator.

The methodology to fabricate the actuator is shown in Fig. 2 (b). The initial step involves creating the stiffer top part (Step 1). This is accomplished by casting a $1.7\,\mathrm{mm}$ thick layer of Dragon Skin 30, along with an inextensible fabric sheet, on top. In Step 2, the manufacturing of the main body of the actuator begins with the first layer, which consists of a cylindrical hollowed Ecoflex 00-30 silicone chamber measuring $54\,\mathrm{mm}$ in width. The chamber is moulded directly onto the stiffer top part, with an inner diameter and height of $50\,\mathrm{mm}$. Step 3 involves applying a two-way stretch fabric around the first layer. The fabric is securely held in place by wrapping the inextensible fibre around the outer surface. By stitching the inextensible fabric to the fibre, a robust connection between the reinforcements is established. Simultaneously, in a separate moulding step, similarly to Step 1, the bottom part is manufactured. This involves placing another inextensible fabric cutout with a diameter of $45\,\mathrm{mm}$ into a $50\,\mathrm{mm}$ mould and pouring the stiffer Dragon Skin 30 silicone material on it. Step 4 involves the sealing of its inner chamber. This is achieved by attaching a 3 mm thick silicone cap at the bottom of the actuator. The cap, whose fabrication process is similar to that outlined in Step 1, is designed to ensure airtight sealing and to facilitate the integration of the pressure pipe. The actuator's fabrication is finalised with an additional layer of Ecoflex 00-30 silicone. This secondary coating is applied to comprehensively envelop the underlying two-way-stretch fabric and the fibre reinforcement. The incorporation of this layer enhances the structural integrity of the actuator and results in an increase in its external dimensions, expanding its outer diameter to $58\,\mathrm{mm}$ and elevating its height to $60\,\mathrm{mm}$.

B. Analytical mathematical model for the SPA

To facilitate the actuator design process, an analytical model is utilised. This approach enables, for instance, achieving the required displacement and force for effective signal transfer through the seat cover to the driver. Additionally, the model ensures the attainment of targeted force outputs which should be between the detection threshold and the threshold that determines pain, approximately $47.1\,\mathrm{N/cm^2}$ for female and $71.6\,\mathrm{N/cm^2}$ for male users, as cited in [42], given size requirements for the actuator's size to embed multiple actuators into the driving seat. The modelling approach, presented in this section, reduces thereby the need for extensive prototyping incorporating the material behaviour under applied pressure, along with the stress distribution within the material. Then, a mathematical representation of the longitudinal strain experienced by the material is provided. This is followed by an

examination of the resistance force generated by the actuator. Fig. 3 provides a schematic representation of the notations used in the equations discussed subsequently.

1) Analytical modelling of stresses: The analytical description of the actuator is based on the work in [28], in which a model for a soft fibre-reinforced flexural actuator was developed. Instead of employing the Neo-Hookean material model [34], the Gent hyperelastic material model is utilised [35]. The Gent model is an enhancement of the Neo-Hookean model which incorporates a defined maximum value to limit the first strain invariant. This model is better suited for the actuator taking into consideration that it can accurately capture the limited extensibility of the two-way stretch fabric utilised in the actuator design. The strain energy is thus given in (1).

$$W = -\frac{\mu J_m}{2} \ln\left(1 - \frac{I_1 - 3}{J_m}\right), I_1 < J_m + 3. \tag{1}$$

I_1 is the first invariant of the three eigenvalues λ_1, λ_2 and λ_3 (axial, circumferential, and radial) as in (2).

$$I_1 = \lambda_1^2 + \lambda_2^2 + \lambda_3^2. \tag{2}$$

The shear modulus μ of the material and J_m, the limit of $I_1 - 3$, are material-specific parameters of the model. For $J_m \to \infty$ the Gent model reduces to the Neo-Hookean model [36].

Due to the incompressibility of the material, Eqn. (3) yields.

$$\det(F) = \lambda_1 \cdot \lambda_2 \cdot \lambda_3 = 1. \tag{3}$$

F is the deformation gradient. The fiber reinforcement of the actuator prevents expansion along the circumference, which leads to negligible strain in the circumferential direction ($\lambda_2 = 1$). For $\lambda_1 = \lambda$, the eigenvalues can be written as in (4).

$$\lambda_1 = \lambda,\ \lambda_2 = 1,\ \lambda_3 = \frac{1}{\lambda}. \tag{4}$$

The Cauchy stress tensor $\boldsymbol{T}$ for the incompressible Gent model is calculated by (5).

$$\boldsymbol{T} = -p\ \boldsymbol{I} + 2\ \frac{\partial W}{\partial I_1}\ \boldsymbol{B} = -p\ \boldsymbol{I} + \frac{\mu J_m}{J_m - I_1 + 3}\ \boldsymbol{B} \tag{5}$$

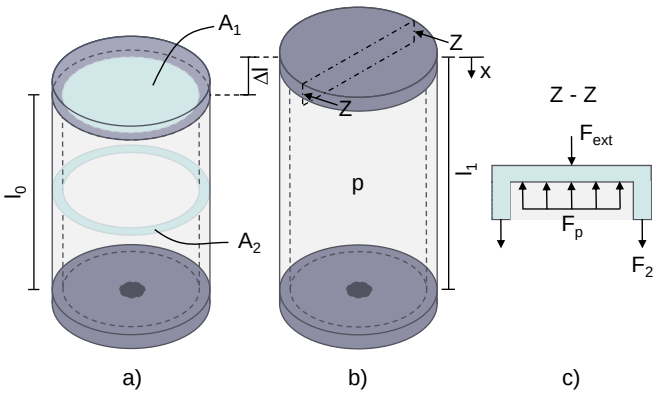

Fig. 3. Sectional view of the actuator a) in the non-actuated state and b) in the elongated state including c) a cutout to describe the acting forces.

Where p is a hydrostatic pressure term representing the incompressibility constraint and $\boldsymbol{B}$ is the left Cauchy-Green deformation tensor [36], which can be expressed as in (6).

$$\boldsymbol{B} = \lambda^2\ \mathbf{n}_1 \otimes \mathbf{n}_1 + \mathbf{n}_2 \otimes \mathbf{n}_2 + \frac{1}{\lambda^2}\ \mathbf{n}_3 \otimes \mathbf{n}_3 \tag{6}$$

This results in the following relationships in (7) - (9) for the three principal stresses.

$$t_1 = -p + \frac{\mu J_m}{J_m - I_1 + 3}\lambda^2 \tag{7}$$

$$t_2 = -p + \frac{\mu J_m}{J_m - I_1 + 3} \tag{8}$$

$$t_3 = -p + \frac{\mu J_m}{J_m - I_1 + 3}\frac{1}{\lambda^2} \tag{9}$$

Due to the thin wall of the actuator with a wall thickness of $4\,\mathrm{mm}$, the radial stress can be neglected ($t_3 = 0$). Consequently, p can be written as in (10).

$$p = \frac{\mu J_m}{(J_m - I_1 + 3)}\frac{1}{\lambda^2} \tag{10}$$

If strains of $1 \leq \lambda < 1.5$, which are reasonable for this application, are considered, the tangential stress t_2 is significantly smaller than the axial stress t_1 ($t_2 < t_1/2$) and thus, as in [28], negligible. t_1 is written as σ. Combining (7) with (2) and (4) yields (11).

$$\sigma = t_1 = (\lambda^2 - \frac{1}{\lambda^2})\frac{\mu J_m}{J_m - (\lambda^2 + 1 + \lambda^{-2}) + 3}. \tag{11}$$

2) Analytical description of the longitudinal strain: Fig. 3 shows the parameters of the actuator required for the calculations of the longitudinal strain. l_0 represents the initial length of the actuator, measured as the height of the inner chamber. The area A_1 is the circular top surface of the chamber and A_2 is the cross-section of the actuator wall. When the actuator is pneumatically pressurised, the internal relative pressure p results in a change in length Δl with respect to l_0. The height of the part of the actuator filled with air is thus given by (12).

$$l_1 = l_0 + \Delta l. \tag{12}$$

The pressure acting on the surface A_1 inside the chamber causes the actuator to elongate and thus the stress σ in the stretched silicone material of the sidewall. At equilibrium, the force F_p arising from the pressure is equal to the force F_2 resulting from the stress due to the elongation of the sidewall. Thus σ can be determined in (13).

$$\sigma = \frac{F_p}{A_2} = p\frac{A_1}{A_2}. \tag{13}$$

By elongating, the cross-sectional area A_2 decreases, which can be described by the initial cross-sectional area $A_{2,0}$ in (14).

$$A_2 = \frac{A_{2,0}}{\lambda} = \frac{(r_a^2 - r_i^2)\pi}{\lambda} \tag{14}$$

Combining (13) and (14) with the relationship already established for σ in (11), Eqn. (15) yields.

$$p = \frac{A_{2,0}}{A_1}\frac{\mu J_m}{J_m - (\lambda^2 + 1 + \lambda^{-2}) + 3}\left(\lambda - \frac{1}{\lambda^3}\right). \tag{15}$$

Considering $\lambda = 1 + \epsilon = 1 + \frac{\Delta l}{l_0}$ results in the relationship between the pressure inside the actuator and the elongation of the actuator. Rearranging this equation, the force F_2 inside the walls of the actuator is obtained in (16).

$$F_2 = A_{2,0} \frac{\mu J_m}{J_m - \left(\left(1 + \frac{\Delta l}{l_0}\right)^2 + 1 + \left(1 + \frac{\Delta l}{l_0}\right)^{-2}\right) + 3} \cdot \left(\left(1 + \frac{\Delta l}{l_0}\right) - \left(1 + \frac{\Delta l}{l_0}\right)^{-3}\right). \quad (16)$$

3) Analytical description of the resistance force: The following explanations examine the relationship between an externally acting force on the tip of the actuator and the resulting deformation. This allows a relationship to be established for the stiffness. Assuming a state of equilibrium, Eqn. (17) results.

$$F_p = F_{ext} + F_2(x). \quad (17)$$

The force F_2 depends on the deformation in the $x-$direction (see Fig. 3 (b)) due to the additional external force since this reduces the strain in the silicone sidewall and thus the stress, as described in (18).

$$F_2 = A_{2,0} \frac{\mu J_m}{J_m - \left(\left(1 + \frac{\Delta l - x}{l_0}\right)^2 + 1 + \left(1 + \frac{\Delta l - x}{l_0}\right)^{-2}\right) + 3} \cdot \left(\left(1 + \frac{\Delta l - x}{l_0}\right) - \left(1 + \frac{\Delta l - x}{l_0}\right)^{-3}\right) \quad (18)$$

The pressure inside the actuator is calculated in (19).

$$p = \frac{F_{ext}}{A_1} + \frac{F_2(x)}{A_1} \quad (19)$$

The top of the actuator is assumed to be a rigid body due to the added reinforcements. The ideal gas law in (20) is applied.

$$p_{abs} V = m R_s T \quad (20)$$

The actuator is assumed to be sealed and the volume in the connected silicone tubes is neglected. Therefore, the volume can be calculated by $V_1 = l_1 \cdot A_1 = (l_0 + \Delta l) \cdot A_1$. Further assuming that the temperature inside the actuator remains constant due to the slow deformation ($T = T_0$), the mass m_1 of the air inside the actuator can be calculated by (21).

$$m_1 = \frac{(p_1 + p_{atm}) V_1}{R_s T_0} \quad (21)$$

Here, the specific gas constant $R_S = 287.05\,\mathrm{J/(kgK)}$ is used. p_1 describes the applied pressure (for elongation) without an external force. When the external force is applied, the volume inside the actuator decreases as in (22).

$$V(x) = (l_1 - x) A_1 \quad (22)$$

The pressure in (23) inside the actuator also depends on the deformation of x and results from the combination of (22) and the ideal gas law (20).

$$p(x) = \frac{m_1 R_s T_0}{(l_1 - x) A_1} - p_{atm} \quad (23)$$

By equating (19) and (23) and transforming the equation according to the external force, (24) is obtained.

$$F_{ext} = \frac{m_1 R_s T_0}{(l_1 - x)} - p_{atm} A_1 - F_2(x) \quad (24)$$

Numerical solving methods offer a means to calculate the deformation (x) of the actuator when subjected to a specific load (F_{ext}). Furthermore, by examining the relationship between force and strain, valuable insights can be gained regarding the actuator's stiffness or resistance. The stiffness can be determined using (25), which relates the applied force and the resulting strain.

$$Stiffness = \frac{F_{ext}}{\epsilon} = \frac{F_{ext} l_1}{x} \quad (25)$$

C. Comparison of experimental and computational characterisation results

To determine the material parameters for the Gent model, as discussed in Section III-B, a tensile test was conducted on the two-way stretch fabric used in the actuator. A specially designed 3D-printed testing jig was utilised to replicate the bi-axial tension experienced by the fabric in the actuator. The testing jig included overlapping walls to prevent fabric necking. During the tensile test, the force applied to the fabric was measured as a function of elongation. The measured data was then fitted with Eqn. (16) using a nonlinear least-squares solver (specifically, the trust-region reflective algorithm) in MATLAB. Initial values of $\mu_0 = 0.15\,\mathrm{MPa}$ and $J_{m,0} = 0.5$ were used, and only positive values were considered. The fitting process resulted in the extraction of the fitted shear modulus $\mu_{fit} = 0.012\,72\,\mathrm{MPa}$ and the fitted strain limit $J_{m,fit} = 0.3179$ for the two-way stretch fabric. To account for the stiffness of the silicone material (Ecoflex 00-30), its shear modulus $\mu_{eco30} = 0.025\,32\,\mathrm{MPa}$ [28] was added to the fitted shear modulus μ_{fit} of the two-way stretch fabric.

However, the two-way stretch fabric shows negligible resisting forces if the length of the actuator is smaller than its initial length l_0 ($\Delta l < 0$). Therefore, the model uses $J_m = 10,000,000 \approx \infty$, which reduces the model to a Neo-Hookean model and $\mu = \mu_{eco30}$ for $\Delta l < 0$.

To validate the model and define the actuation parameters, a series of three experiments were conducted, each confirming a key feature of the actuator's intended use in a haptic feedback driver seat (i.e., elongation behaviour, force generation capability, and stiffness adaptability). To measure the elongation, the actuator is equipped with small black marker stickers (see Fig. 4) and recorded with a digital camera (Sony, Alpha 7). The videos were analysed using a computer vision algorithm that tracks the markers. Forces were measured using a universal testing machine (ZwickRoell Z2.5) with a $500\,\mathrm{N}$ load cell (ZwickRoell Xforce P, 057993).

1) Actuator elongation: Preliminary tests have shown that actuation to 10 mm by a single actuator results in a clearly perceptible haptic signal. According to the analytical model, this elongation can be achieved without any external force by applying a pressure of $15\,\mathrm{kPa}$. To validate the model and ensure its accuracy, the actuator's elongation was measured

using a video extensometer while incrementally increasing the applied pressure up to 25 kPa. Fig. 4 presents the results showing the measured elongation at a pressure in red colour with the error deviation in the red shaded colour and the model in blue colour. The applied pressure vs. elongation curve increases logarithmically. Both, the measured elongation closely aligns with the predictions from the analytical model. The required 10 mm are in fact achieved at 15 kPa, while the maximum applied pressure of 25 kPa leads to an elongation of 12.2 mm. The observed curves display minimal deviations. These deviations may arise from minor dimensional discrepancies between the actual actuator and the geometry specified in the model, potentially due to manual manufacturing processes. Additionally, the deviations can be partly attributed to uncertainties in measuring material properties and the elongation of the actual actuator. The use of the Gent model, which offers only a limited representation of material properties, may also contribute to these discrepancies.

2) Generated forces: In addition to the required elongation for effective signal transfer, it is essential for the actuator to generate an adequate force that can capture the driver's attention. To verify the model's ability to accurately describe the relationship between force and applied pressure, the actuator was pressurised while restricting elongation, and the resulting force at the top surface was measured. Fig. 5 presents the results of this experiment (average value in the red coloured curve with error deviation in a shaded red colour) and the simulation (in the blue coloured curve). Both curves show a linear relationship. The observed behaviour aligns well with the modelled behaviour. It is worth noting that a force output of up to 50 N is considered sufficient for reliably transmitting haptic signals while remaining below the human back's pain threshold [42]. This is due to the actuator's relatively large contact area of 26.4 cm^2, which helps distribute the force and minimise discomfort.

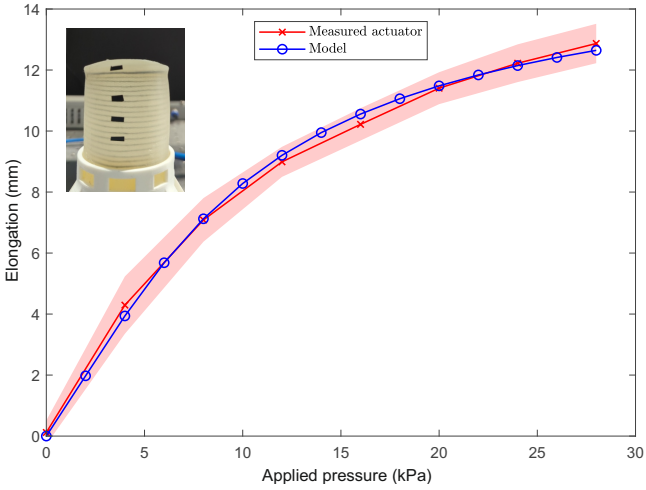

Fig. 4. Results of the actuator elongation: Measured elongation of the actuator tip over pressure compared with the computational model. Measurements of six trials (using the same actuator in each trial) were captured by a video extensometer with passive markers. The setup is shown in the top left.

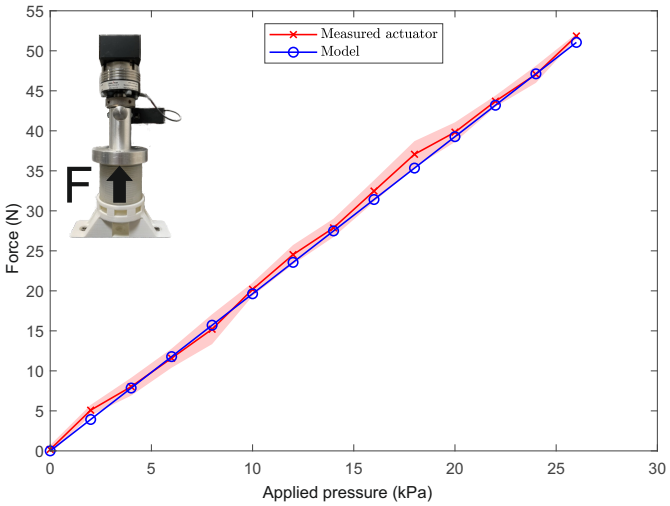

Fig. 5. Results of the generated forces: Force measured at the top surface of the actuator (x-direction) over applied pressure while preventing actuator elongation (blocked force tests). Experimental setup is shown in the top left and tests are repeated five times, using the same actuator in each trial.

3) Adaptable stiffness: To ensure minimal driver discomfort and imperceptibility of the actuators in the seat when inactive, it is important to customise the stiffness of the actuators. The stiffness can be adjusted by controlling the pressure within the actuators when there is no actuation. To investigate this, the resistance force against compression was measured for both a closed tube and an open tube, where no external pressure was applied. Fig. 6 illustrates the results of the experiments and simulations. The pink curve represents the case of an open valve, where air can escape from the actuator through the pipe. The red curve corresponds to the case of a closed valve, where

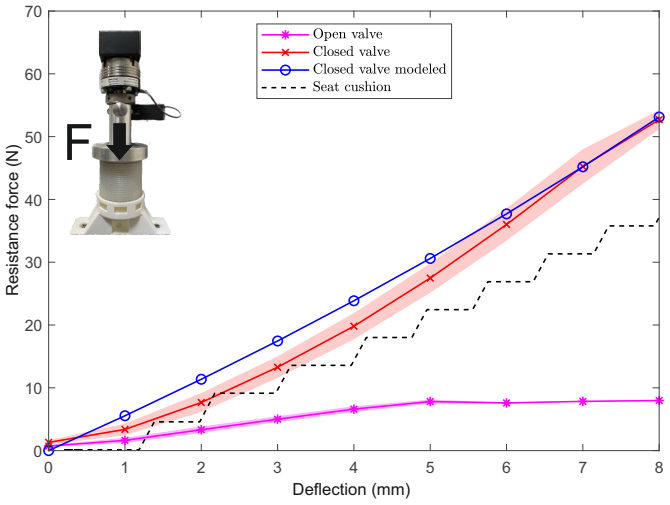

Fig. 6. Results of the adaptable stiffness: Resistance force for a deflection of 8 mm while no external pressure is applied. Open valve (pink colour), i.e., air can escape from the actuator. The actuator walls start to buckle at 5 mm deflection. Closed valve (red colour), i.e., the air pressure inside the actuator increases during loading as no air can escape from the actuation chamber. The actuator does not collapse due to the inner pressure. Experimental setup is shown in the top left and tests are repeated five times, using the same actuator in each trial. The data for the seat cushion originates from Zhang et al. [46].

the air pressure inside the actuator increases during loading as no air can escape from the actuation chamber. The shaded area represents the error deviation for both experimental results. The computational results for a closed valve are presented in blue. In the case of an open valve, the resistance force remains below 9 N. At a deflection of approximately 5 mm, indicated by the change in slope of the linear curve, the actuator starts to buckle. Conversely, in the case of a closed valve, the pressure inside the actuation chamber increases during compression loading, preventing the actuator from buckling.

Since the actuator length is smaller than the initial length l_0 in this experiment, the influence of the two-way stretch fabric was neglected in the model as described at the beginning of Section III-C. Both the experimental and simulation deflection-force curves show a slow exponential increase. The model, however, overestimates the forces for a deflection of 1 to 5 mm with a maximum offset of 4.17 N. One reason for this discrepancy might be that the material properties in the model were measured during tensile loads. In addition, the fibre reinforcement, while mitigating the ballooning effect, does not entirely eliminate it. This partial mitigation can lead to a minor increase in volume, consequently resulting in reduced force measurements for the actuator when the valve is closed.

The stiffness of the seat cushion, as quantified by Zhang et al. [46], falls between the stiffness levels of the actuator with a closed valve (being less stiff) and the actuator with an open valve (being more stiff). Within the examined region, the force-deflection curve exhibits an almost linear trend, suggesting a consistent stiffness.

D. Rise time and frequency response

The performance of the soft actuator was characterised in terms of its rise time and frequency response. The evaluation employed an array of five infrared cameras (OptiTrack, Prime 17W) operated via a MATLAB/Simulink framework as described in [47]. To facilitate precise tracking, five passive infrared markers were affixed on the top of the actuator, which was subsequently subjected to a pressure of 20 kPa. Analysis of the actuator's dynamic response revealed that, for a 10 mm elongation, the rise time from 10% to 90% was recorded at 0.127 s (SD = 0.0086 s) across ten iterations. Similarly, the fall time was computed using an analogous approach, resulting in a duration of 0.241 s (SD = 0.0038 s). Consequently, the actuator demonstrated a frequency response capability of 2.72 Hz.

IV. Embedding Soft Robotic Actuators into a Driver Seat

Based on the findings from Section III, a soft robotic, haptic feedback seat based on a 2019 Land Rover Discovery Sport SE driver seat was created. The seat has a 2 mm genuine leather seat cover with a 8 cm to 14 cm foam underneath. Twelve soft robotic actuators are embedded in the foam under the cover. Eight actuators are located in the bottom side bolsters and four are integrated into the back side bolsters of the seat, as shown in Fig. 7. The side bolsters offer sufficient space for the actuators and are less pressurised by the weight of the driver. Also, signals in the side cushions are perceived as more pleasant compared to signals in the bottom of the seat [30].

A. Haptic feedback areas

Fig. 7 (a) illustrates the configuration of two designated haptic feedback areas (HFA) and the location of the actuators. HFA 1 is utilised to transmit signals in the direction of travel (see Fig. 7 (a), x-direction), while HFA 2 serves to assist the driver in distinguishing between the left and right sides, i.e., in the positive or negative y-direction. Within the bottom side bolsters (HFA 1), there are a total of eight actuators, with four actuators labelled LLX on the left side and four actuators labelled LRX on the right side, where $[X = 1, ..., 4]$. To regulate the pressure of all HFA 1 actuators, four pressure regulators are employed. Each LLX/LRX pair of actuators is pressurised by a single regulator. In the area HFA 2, i.e., signals that refer to the left or right side of the vehicle, the two actuators on each side are pressurised by one valve each.

The two-point contact threshold which determines the spatial resolution on the human skin is 40 mm for the legs and 45 mm for the back [31]. A distance of 60 mm between the centres of the actuators was chosen to guarantee the haptic area of the seat covering a wide range of possible human body sizes and seating positions.

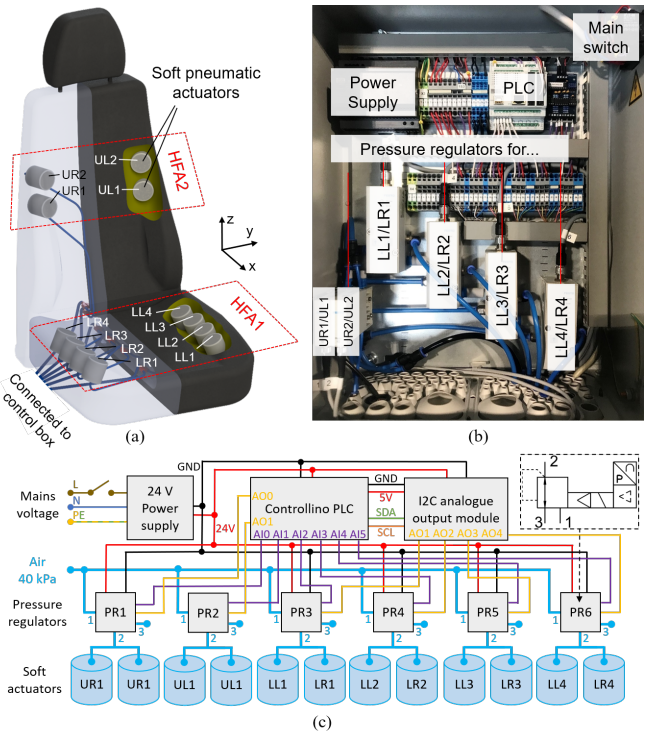

Fig. 7. (a) The haptic feedback seat with twelve integrated soft pneumatic actuators. In the area HFA 1, eight soft robots are embedded, four on each side labelled LLX on the left and LRX with $[X = 1, ..., 4]$ on the right side. In the area HFA 2, two actuators are placed on each side. (b) The actuators are connected to a control box with a programmable logic controller (PLC) connected to pressure regulators. The pressure of all HFA 1 actuators is controlled by four pressure regulators, where an LLX/LRX pair is pressurised by one regulator. The pressure for HFA 2 is controlled by another two regulators in the same way. (c) An electrical and pneumatic circuit diagram of the system. The PLC sets the target pressure values for the pressure regulators by an analogue signal (yellow) and receives analogue values of the real pressure (violet). The pressure regulators are interfaced pneumatically via an air inlet (1), an air outlet (2) and an exhaust (3). The pneumatic functionality of the pressure regulators is shown in the upper right corner [32].

B. Actuation patterns

The eight actuators installed in HFA 1 are used to generate wave-like signals within the driver seat bottom. For this purpose, the actuators on the left and right sides are activated for a short time, after which the next actuators are actuated. For a wave running backwards from the driver's point of view, the actuator pair LR1/LL1 is actuated first until LR4/LL4 are finally actuated. When a pair is actuated, the adjacent pairs are activated with lower pressure. For example, at the beginning of the wave, when LR1/LL1 is actuated, the next pair LR2/LL2 is actuated with a lower pressure too. In step two, LR2/LL2 is then fully actuated while LR1/LL1 and LR3/LL3 are set to the lower pressure. This results in an overlapping wave. Overlapping waves, similar to a "stadium wave", are perceived as more pleasant by subjects as shown by Petermeijer et al. [37]. A wave running in the opposite direction of travel is supposed to give the driver the feeling that something is coming towards them and that they need to take control. The dynamics of the signal are used to convey a certain urgency. In [38], Lewis et al. investigated how pulse duration of different lengths, i.e., the time during which the actuators are active, affects perceived urgency. They found that a pulse duration of $150\,\mathrm{ms}$ was able to convey the highest urgency. With each pair actuated for $150\,\mathrm{ms}$, the total time needed for one wave is $600\,\mathrm{ms}$. The actuation pressures are chosen in accordance with the analytical model described above. Preliminary tests showed that an elongation of $12\,\mathrm{mm}$ resulted in a clear but still comfortable haptic signal. In order to get an elongation of $12\,\mathrm{mm}$, a pressure of $23.0\,\mathrm{kPa}$ is set as the wave peak actuation pressure. The adjacent actuator pairs in the wave pattern are pressured with $11.5\,\mathrm{kPa}$.
HFA 2 is used to transmit signals that are intended to direct the driver's attention to the left or right or to inform about dangers on the left/right side. For the control take-over requests caused by obstacles in the direction of travel investigated in this study, the actuators in HFA 2 are only actuated in a supportive manner. For this purpose, the actuators are actuated at $20\,\mathrm{kPa}$ for $600\,\mathrm{ms}$ in sync with the wave actuation of HFA 1.

C. Interfacing the array of Soft Pneumatic Actuators

The control box used to actuate the soft pneumatic actuators inside the haptic feedback seat as well as the electrical and pneumatic circuit diagram of the system are shown in Figs. 7 (b) and (c). A programmable logic controller (PLC) (Conelcom GmbH, Controllino Maxi Automation) is connected via I2C-bus and an analogue output module to the two different kinds of proportional pressure regulators used in this study. The actuators in the bottom seat (LR1-4, LL1-4) are operated by proportional pressure regulators of the type VPPM (Festo, VPPM-6L-L-1-G18-0L2H-V1P-S1) for fast and dynamic pressurisation, while the actuators in the upper part of the seat (UR1-2, UL1-2) are actuated with smaller proportional pressure regulators (Festo, VEAB-L-26-D2-Q4-V1-1R1). To eliminate noise, the exhaust air connections of the VPPM and VEAB valves are equipped with silencers (Festo, UC-1/8 or UC-QS-4H). Besides controlling the actuators, the PLC is handling user inputs like the emergency and reset buttons. The pneumatic and electronic parts are separately kept in a control box to prevent any noise that could interfere with the studies.

V. Experimental setup and protocol

Section V-A describes the driving simulator platform that was built for this research study. Implemented driving scenarios for the experiments with participants are detailed in Section V-B. A total of three experiments have been conducted to assess the acceptance (separated into usefulness and satisfaction) and usability of the haptic feedback seat (see Section V-C and V-D). The results of all experiments are presented in Section VI and discussed in Section VII.

A. Description of the driving simulator - experimental setup

Figure 1(a) illustrates the driving simulator setup. The central component of the configuration is the haptic feedback seat, featuring integrated soft actuators positioned according to the details provided in Section IV-A. Positioned in front of the seat are a steering wheel and foot pedals (Logitech, G29 Driving Force). These elements, along with an emergency button, control box, and power supplies, are all mounted to a honeycomb optical table. Displaying the driving scenarios is a 65-inch screen (Legamaster). To allow for participants' individual driving preferences, the seat, screen, steering wheel, and foot pedals can be adjusted horizontally and vertically. For auditory immersion in the driving scenarios and audible takeover requests, a Razer Kraken X 7.1 headset is employed.

B. Driving scenarios with take-over requests

The driving scenarios for the experiments have been designed using the simulation software Beam.NG. The package is based on the Torque Game Engine and uses *Soft Body Physics* to simulate detailed driving behaviour of vehicles. The simulations are executed on a PC with an AMD Ryzen 5 3600 processor and a Radeon RX5700 XT graphics card, delivering a 1080p Full HD display.

All the driving scenarios are captured from the driver's view. The alignment of the steering wheel in the simulation mirrors that of the physical steering wheel in the driving simulator, achieved by adjusting the positioning of the monitor and steering wheel themselves. The duration of these scenarios varies, ranging between $27\,\mathrm{s}$ and $73\,\mathrm{s}$. To prevent participants from anticipating impending takeover requests, a mix of shorter and longer scenarios is employed.

At the beginning of the scenarios, the vehicle operates in level-3 autonomy, navigating a multi-lane motorway for between $23\,\mathrm{s}$ to $69\,\mathrm{s}$ as shown in Fig. 8 (a). Then, a TOR informs the driver to take back control as a number of static vehicles and obstacles are placed on the motorway at the end of the scenarios to represent, e.g., a traffic jam (Fig. 8 (b)), an accident (Fig. 8 (c)), obstacles on the road (Fig. 8 (d)), and a police checkpoint (Fig. 8 (e)). The vehicle will require the human participant to take over control of the vehicle (i.e., autonomy level 0) to successfully manage these parts of each scenario. The take-over request is signalised using audio or haptic feedback using the seat.

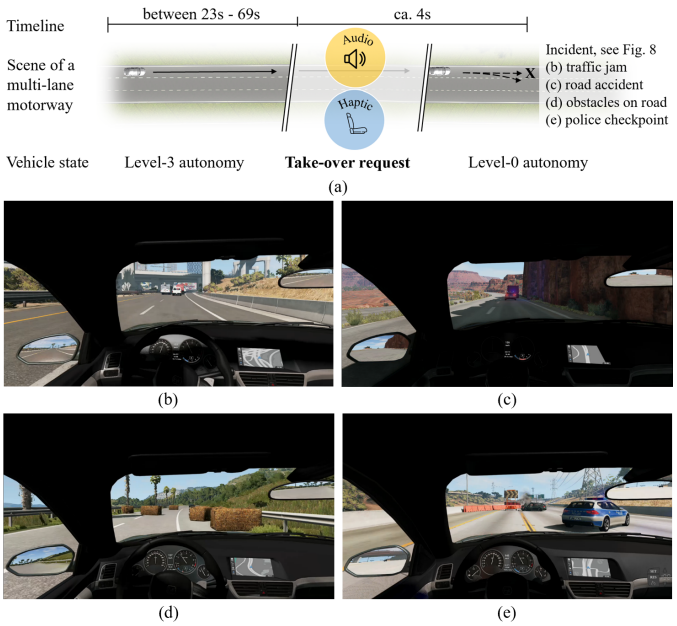

Fig. 8. (a) Overview of the scenarios. Participants will experience driving along a multi-lane motorway in level-3 autonomy for a duration of 23 s to 69 s. Then, audio or haptic feedback is given to the participant, indicating to take over control due to (b) a traffic jam, (c) a road accident, (d) obstacles on the road and (e) a police checkpoint.

C. Evaluation methodology of the haptic feedback seat

Through a set of questionnaires, the acceptance, which is classified into usefulness and satisfaction, as well as the system's usability with regards to the haptic feedback seat is evaluated by each participant. The assessment tools utilised in this study include the acceptance assessment by Van der Laan et al. [29]. On the other hand, the usability test is based on the work by Brooke [33]. These tools were selected for their high content validity, thoroughly discussed and supported by Foster et al. [39].

Acceptance of the driver seat: Following the evaluation protocol outlined by Van der Laan et al., an analysis of driver acceptance concerning the haptic feedback seat is undertaken. Participants are asked to provide their assessment on a scale spanning from -2 to $+2$, both prior to and after engaging with the driving scenarios, to determine differences in expected and actual acceptance. These assessments are termed pre- and post-measurements, respectively. The feedback will help to understand if the haptic feedback seat is (1) useful/useless, (2) pleasant/unpleasant, (3) bad/good, (4) nice/annoying, (5) effective/superfluous, (6) irritating/likeable, (7) assisting/worthless, (8) undesirable/desirable, and (9) raising alertness/sleep-inducing. Conclusions with regards to the usefulness are made by analysing statements 1, 3, 5, 7, and 9 while the satisfaction is measured through the remaining statements 2, 4, 6, and 8. Statements 3, 6, and 8 are mirrored to avoid participants answering in patterns. Further details are provided in Appendix A.

Usability of the driver seat: To facilitate the assessment of system usability, the study employs the System Usability Scale as outlined in the work by Brooke. This method comprises a set of ten questions designed to compute the System Usability Score (SUS). In contrast to alternative systems, this score offers insights into the degree to which the system under examination is perceived as user-friendly. Participants express their perspectives on usability using a Likert scale that spans from "agree", "rather agree", "partly agree", "rather disagree" to "disagree". Appendix B includes details on the SUS questionnaire.

D. Experimental protocol

Experiment 1: The first experiment serves the purpose of familiarising participants with the system and the tactile sensations delivered through the haptic feedback mechanism. Following the completion of a data privacy statement and consent form, participants are asked to take a seat in the driver's chair and make necessary adjustments to ensure comfort. To introduce them to the capabilities of the haptic feedback, the four soft actuators located in HFA2 (UL1-2, UR1-2) of the seat are activated four times. Each activation persists for a duration of $1\,\mathrm{s}$, with a pressure of $20\,\mathrm{kPa}$ applied. Then, the pressure within each of the eight soft actuators located in the bottom of the seat (LR1-LR4 and LL1-LL4) is gradually elevated to $20\,\mathrm{kPa}$ over a duration of $5\,\mathrm{s}$. This is followed by a demonstration of the wave-like patterns that will subsequently serve as the stimuli for Experiment 2. The actuation lasts for a total duration of $4.8\,\mathrm{s}$. A description and application of the haptic feedback seat is then provided to the participants. They are asked to envision themselves on the driver seat in an automated vehicle that navigates along a highway in full autonomous mode. A scenario arises that requires the participant to interfere and take over control of the vehicle. This control request is initiated via the utilisation of soft pneumatic actuators embedded within the driver seat, offering tactile cues to signal the transfer of control. Following these explanations, participants are tasked with responding to the nine acceptance-related questions (pre-measurement) formulated in accordance with Van der Laan et al. [29].

Participants are then informed about two driving scenarios, they will experience in Experiment 2. They are briefed that their vehicle is equipped with level-3 autonomy features. Lane-keeping, cruise control, and the ability to autonomously overtake other vehicles on highways are activated. An auditory take-over request, similar to the one of a Tesla Model 3 (a sample is included in the supplementary video), might occur when the vehicle requires the participant to take over control and manage a driving incident by promptly engaging the brake pedal. A sample of the audio signal is demonstrated to familiarise participants with the feedback system of commercially available highly automated vehicles.

Experiment 2: Five driving scenarios are presented to the participants, similar to the ones shown after the questionnaire of Experiment 1, with the difference that the take-over request is initiated by the soft actuators and a wave-like pattern of the haptic feedback seat. After Experiment 2, the participants are asked to share their feedback with regards to the same nine questions published by Van der Laan et al. [29] (post-measurement), in addition to the ten questions of the System Usability Scale in the paper by Brooke [33].

E. Participants

Twenty-one participants (8 female; 13 male) with a height of 160 cm to 200 cm (M = 178.6 cm; SD = 10.1 cm) and weight of 55 kg to 115 kg (M = 72.9 kg; SD = 13.8 kg) participated in this study. The participants have an average driving experience of 11.0 years (SD = 5.2 years). Among the participants, four individuals use their cars on a daily basis, while eight individuals utilise their cars weekly. Additionally, three participants indicated a monthly usage frequency. Six participants reported driving less frequently than on a monthly basis. This study has been approved by the UCL Research Ethics Committee (No. 17579/002).

VI. Experimental Results

A. Acceptance of the soft robotic, haptic feedback driver seat

The acceptance results are presented in this section, divided into the assessment of the usefulness and satisfaction. Fig. 9 shows results of the usefulness and Fig. 10 results for the satisfaction in the form of violin plots, a combination of a box and a kernel density plot. Pre-measurements (Experiment 1) are shown in red colour and post-measurements (Experiment 2) in blue colour. The violin sub-plots on the right-hand side in each figure show the overall usefulness and satisfaction, respectively. To validate the internal consistency of the questionnaire, Cronbach's alpha is calculated for both acceptance components (i.e., usefulness and satisfaction) using the statistical software package IBM SPSS.

1) Usefulness: For the five questions related to the usefulness of the haptic feedback seat, Cronbach's alpha is 0.748 for the pre-measurement, which is above the threshold of 0.65. Therefore, the questions can be considered sufficiently consistent to determine the usefulness of the system. As seen in Fig. 9, each post-measurement of usefulness-related questions achieved a higher rating compared to the corresponding pre-measurement. Overall, pre-measurements resulted in a mean rating of 1.18 (SD = 0.23 for cross-question and SD = 0.62 for cross-subject), with the highest value of 1.43 (SD = 0.87) for Question 7 (Assisting) and the lowest value of 0.86 (SD = 0.85) for Question 5 (Efficient). Post-measurements on the other hand yield in an overall rating of 1.65 (SD = 0.09 for cross-question and SD = 0.50 for cross-subject), with Question 9 (Raising alertness) resulting in the highest rating (M = 1.76, SD = 0.54) and Questions 5 (Efficient) and 7 (Assisting) in the lowest rating (M = 1.57, SD = 0.60/SD = 0.60). When comparing pre- and post-measurements, an overall increase of 40 % can be observed. The highest increase can be seen for Question 5 (Efficient) with a difference of 83 % between the pre- and post-measurements. For Question 7 (Assisting), the lowest difference of about 10 % is noted. A Paired T-Test shows that the difference between pre-measurement and post-measurement ratings is statistically significant ($t(20) = -3.56, p = .002$), as $|t(20)| > t_{krit}(\alpha, n)$.

2) Satisfaction: Cronbach's alpha for the five questions related to understand the satisfaction of the haptic seat in Fig. 10 is 0.599 for the pre-measurement, which is below the threshold of 0.65. Excluding Question 4, however, returns a Cronbach's alpha value of 0.665 for the pre-measurement. Hence, the results for the satisfaction of the system is sufficiently consistent to measure satisfaction with the system, when Question 4 is excluded. To maintain comprehensiveness, Question 4 is still illustrated in Fig. 10, but not included in the satisfaction assessment. Similar to the results for the usefulness, each post-measurement of satisfaction-related questions achieved a higher rating compared to the corresponding pre-measurement in Fig. 9. For the pre-measurement, an overall satisfaction mean value of 1.00 (SD = 0.10) is calculated. Question 8 (Desirable) yields the highest rating (M = 1.10,

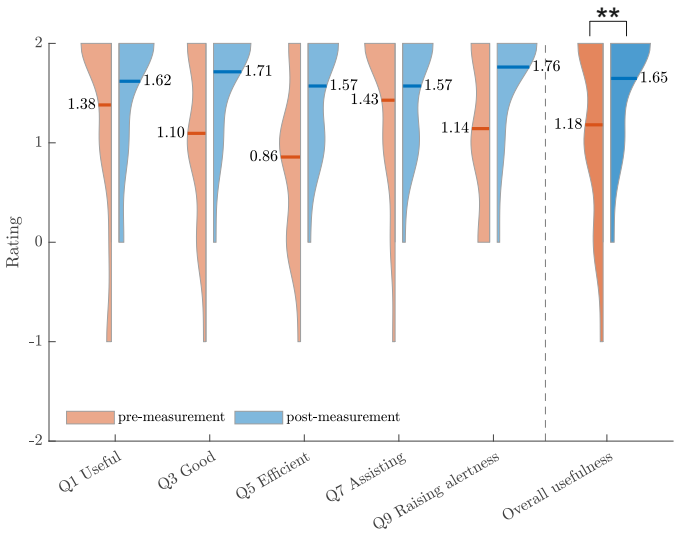

Fig. 9. Results for the usefulness: Violin plots show the pre-measurements (Experiment 1) in red colour and post-measurements (Experiment 2) in blue colour. The plot on the right-hand side gives the overall usefulness. Each post-measurement achieved a higher rating compared to the corresponding pre-measurement.

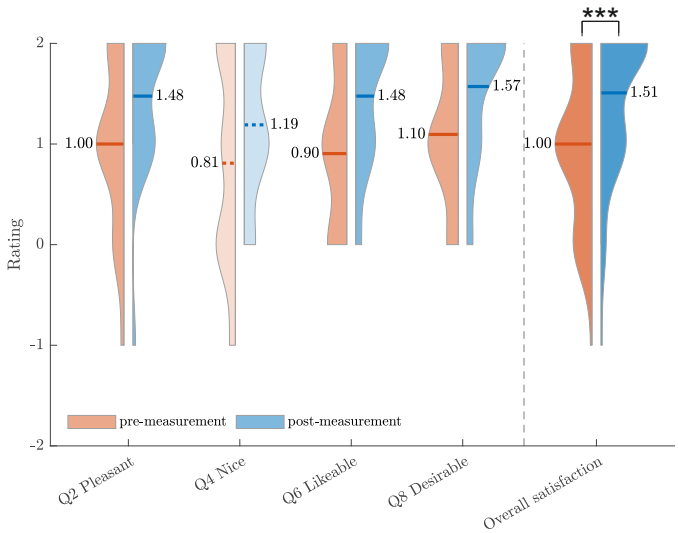

Fig. 10. Results for the satisfaction: Violin plots show the pre-measurements (Experiment 1) in red colour and post-measurements (Experiment 2) in blue colour. The plot on the right-hand side gives the overall usefulness. Note: Question 4 is removed for calculating overall satisfaction but shown for completeness.

SD = 0.70). Question 6 (Likeable), on the other side, has the lowest rating (M = 0.90, SD = 0.77). The mean overall satisfaction rating in the post-measurement is 1.51 (SD = 0.05 for cross-question and SD = 0.52 for cross-subject). As for the pre-measurement, Question 8 (Desirable) yields the best rating after the experiment (M = 1.57, SD = 0.68) and Questions 6 (Likeable) has the lowest rating (M = 1.48, SD = 0.68). The highest increase of 63 % in satisfaction can be seen for Question 6 (Likeable). The lowest increase of 44 % is achieved for Question 8 (Desirable). The increase in overall satisfaction between the pre- and postmeasurement is 51 %. Again, a Paired T-Test proves statistical significance for the within-subject evaluation ($t(20) = -5.78,\ p < .001$).

B. Usability of the soft robotic, haptic feedback driver seat

The System Usability Score (SUS) rating for each participant is shown in Fig. 11 between 0 and 100. As the initial questionnaire asked for a rating between 1 and 5, the answers have been transferred to a scale from 0 (worst) to 10 (best) first: On the one hand, answers with an odd number (1, 3, 5, 7, 9) are reduced by 1 point and then multiplied by 2.5. On the other hand, questions with an even number (2, 4, 6, 8, 10), for which 1 describes the best possible outcome and 5 the worst, are subtracted from 5 and then multiplied by 2.5. The new ratings were all added up for each participant, creating a final score (the *System Usability Score*) between 0 and 100. As shown in Fig. 11, two participants have given a maximum SUS of 100. The lowest SUS value is 67.5. The soft robotic haptic feedback seat achieved a mean SUS value of 89.67 (SD = 8.81).

As the System Usability Score should not be interpreted as an absolute measure, the results were converted into the method proposed by Bangor et al. [44]. They performed an evaluation based on the averaged SUS values of 974 subjects. The study resulted in a classification of the SUS into seven categories: “worst imaginable” (SUS < 20.3), “awful” (SUS > 20.3), “poor” (SUS > 35.7), “OK” (SUS > 50.9), “good” (SUS > 71.4), “excellent” (SUS > 85.5), and “best imaginable” (SUS > 90.9). As summarised in Table I, 10 participants (equivalent to 48% of all subjects) have given feedback classified as “best imaginable”. Another 10 participants rated the haptic feedback seat in the categories “excellent” or “good”. The mean SUS of 89.67 represents an “excellent” rating in accordance with Bangor et al. [44].

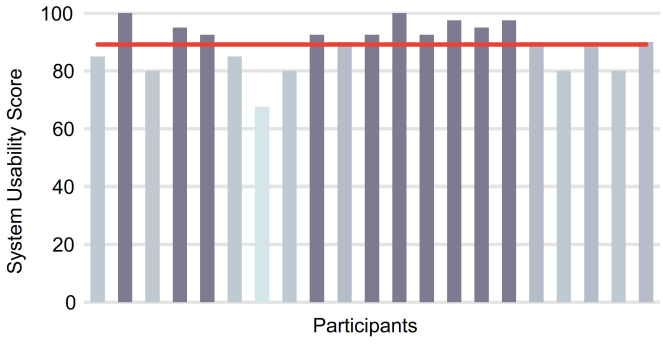

Fig. 11. Results of the System Usability Scale questionnaire rated between 0 and 100: Mean System Usability Score of 89.67 indicated in red colour.

TABLE I
CLASSIFICATION OF SUS VALUES IN ACCORDANCE WITH [44].

Classification by [44]	Best imaginable	Excellent	Good	OK
Number of participants	10	4	6	1
Percentage	48%	19%	28%	5%

VII. DISCUSSION

A. Acceptance

Drawing upon the findings presented in Figs. 9 and 10, it becomes evident that the overall average rating recorded in Experiment 1 is at least 1 or higher. This suggests a clear inclination among participants towards anticipating a substantial degree of usefulness and satisfaction from the haptic feedback seat. Furthermore, the ratings assigned by participants to the seat after engaging in potential scenarios during Experiment 2 indicate not only the fulfilment of these expectations but also their surpassing.

Experiment 2 also investigated other modalities, i.e., auditory feedback. To offer a comparative context for the results, they are aligned with previous studies: In a study by Forster et al. [39], the research explored the acceptance of a visual-human user interface for TORs within a highly automated vehicle with level-3 autonomy capabilities. The study evaluated various self-reporting metrics to assess human-machine interfaces in automated driving, utilising distinct visual displays. The authors employed the dashboard of a BMW Series 5, wherein the visual cues were adaptations and combinations of the signals from the commercially available BMW interface. The outcomes of their study revealed a mean rating ranging from 0.73 to 1.24 points for usefulness and 0.57 to 1.24 points for satisfaction for various visual feedback.

In another study carried out by Fabienne Roche and Stefan Brandenburg, the acceptance of various TORs in a highly automated vehicle was explored, focusing on the integration of combined audio-tactile cues [41]. The signals were conveyed through vibro-tactile stimulation in the seat and a visual cue presented directly on the virtual roadway within the simulator. The research revealed an average rating ranging from 0.75 to 1.39 points for usefulness and 0.25 to 0.84 points for satisfaction with their system. These ratings varied based on factors such as handover lead time and signal urgency. It’s worth noting that the utilisation of vibro-tactile signals in the study might contribute to the slightly lower satisfaction scores, despite only moderately affecting the usefulness scores.

A study by Reinmueller et al.investigated negative behavioural adaptation to adaptive forward collision warning systems using a combined audio-visual signal [43]. The study investigated whether signals adapted to the driver’s current situational awareness have a positive effect on the acceptance of the warning system. In line with this study, a forward collision warning system was evaluated by participants through a series of pre- and post-measurements. Perceived usefulness decreased from 1.51 points in the pre-measurement to 0.96 points in the post-measurement. The satisfaction ratings did

not decrease as significantly as the usefulness ratings (pre-measurement 1.13 points, post-measurement 1.01 points). Although the usefulness for the customisable warning system with an audio-visual signal is higher in the pre-measurement than the concept presented here, the perceived usefulness decreases significantly after using the system.

Overall, the proposed haptic feedback driver seat achieved higher ratings in terms of both usefulness and satisfaction in post-measurements compared to pre-measurement results. Also, this technology returns overall means of 1.65 and 1.51, respectively, achieving higher ratings than related previous studies [39], [41], [43].

B. Usability

In the evaluation of usability analysis, it is valuable to refer to related studies within the existing literature. In fact, the visual-human user interface created by Foster et al. [39], introduced in the previous section, also evaluated their system using the System Usability Scale. The study determines a SUS value of 82.5 resulting in a "good" rating.

In another study by Forster et al. [45], the authors investigated audio signals for TOR in highly automated vehicles. 17 participants took part in the study, in which they were presented with generic audio signals (two high-frequency warning tones) and voice-based audio signals, i.e., "Unclear lane ahead, please take over soon.". in combination with generic audio signals. The participant's feedback yielded a mean SUS value of 74.5 for the system with generic audio signals and 91.6 for combined audio signals.

Overall, the haptic feedback seat, with an average SUS score of 89.67, surpasses the usability scores achieved by both visual and audio feedback systems. When considering instructive feedback as explored in the work by Foster et al. [45], the haptic feedback seat resulted in a similar score.

VIII. Conclusions

This paper presented the design and evaluation process of a haptic feedback driver seat. The seat, equipped with an embedded array of soft pneumatic actuators, is capable of informing the driver of a TOR through static mechano-tactile haptic feedback. The evaluation process engaged 21 participants who took part in various experiments within a driving simulator, experiencing both auditory and haptic feedback from the seat. The outcomes of these evaluations showed notably positive results. In pre-measurements, participants displayed considerable acceptance levels (usefulness: 1.18 and satisfaction: 1.00), which were further amplified in post-measurements (usefulness: 1.65 and satisfaction: 1.51). With regards to the usability, the haptic feedback seat achieved an average SUS score of 89.67. A comparison to similar studies in the literature shows that a static mechano-tactile haptic feedback seat has the potential to achieve higher ratings with regards to technology acceptance and usability compared to visual and audio feedback systems.

Moving forward, future work will explore several paths. One such direction involves expanding the participant pool within a full-size driving simulator. Additionally, there is a keen interest in creating a haptic feedback seat that could offer personalised and inclusive feedback to users. In fact, the proposed haptic feedback seat, incorporating multiple embedded soft robotic actuators, offers a diverse range of design and actuation configurations and patterns, such as static mechano-tactile and vibro-tactile actuation. These variables significantly expand the potential applications of the haptic seat beyond just TORs. For instance, one such application could involve informing the driver about objects in the vehicle's blind spots. This can be achieved by specifically activating HFA2 or a similar mechanism within the system. This capability demonstrates the versatility and practical utility of the design in enhancing situational awareness and safety in vehicular environments.

Appendix A
Overview of the acceptance model by Van der Laan et al.

The assessment of the haptic feedback seat involved the acceptance model by Van der Laan et al. [29], often used in the context of evaluating vehicle interface technologies, designed to measure two key dimensions:

- Usefulness: How beneficial the user perceives the technology.
- Satisfaction: The level of pleasure the user experiences while using the technology.

The model involves a questionnaire with nine items with the following interpretations:

1) Question 1 assesses the perceived utility of the system in enhancing driving performance or assisting in driving tasks.
2) Question 2 evaluates the emotional response of the user to the system, focussing on the overall pleasantness of the interaction.
3) Question 3 measures the perceived quality of the system.
4) Question 4 understands the user's experiential satisfaction with the system.
5) Question 5 determines the perceived effectiveness of the system in contributing to driving tasks, as opposed to being unnecessary or redundant.
6) Question 6 captures the level of irritation or frustration experienced by the user, versus the system being agreeable and user-friendly.
7) Question 7 evaluates whether the system is seen as providing valuable assistance in driving or regarded as having no useful contribution.
8) Question 8 reflects the user's preference for having the system as part of their driving experience, indicating its desirability or lack thereof.
9) Question 9 assesses whether the seat enhances situational awareness or conversely, contributes to a decreased awareness.

These questions were presented in a Likert scale format, where users rate their agreement or disagreement with statements related to each of these aspects as shown in Table II. Conclusions with regards to the usefulness are made by analysing Questions 1, 3, 5, 7, and 9 while the satisfaction is measured through the remaining Questions 2, 4, 6, and 8.

TABLE II
QUESTIONNAIRE BY VAN DER LAAN ET AL. PRESENTED IN A LIKERT SCALE FORMAT [29].

Question	The haptic feedback seat designed for TORs is...		
1	useful	☐ ☐ ☐ ☐ ☐	useless
2	pleasant	☐ ☐ ☐ ☐ ☐	unpleasant
3	bad	☐ ☐ ☐ ☐ ☐	good
4	nice	☐ ☐ ☐ ☐ ☐	annoying
5	effective	☐ ☐ ☐ ☐ ☐	superfluous
6	irritating	☐ ☐ ☐ ☐ ☐	likeable
7	assisting	☐ ☐ ☐ ☐ ☐	worthless
8	undesirable	☐ ☐ ☐ ☐ ☐	desirable
9	raising alertness	☐ ☐ ☐ ☐ ☐	sleep inducing

Questions 3, 6, and 8 are mirrored to avoid users answering in patterns. All responses are then analysed to understand overall user acceptance, highlighting areas of strength and potential improvement for the technology in question.

APPENDIX B
USABILITY QUESTIONNAIRE BY BROOKE

The System Usability Scale (SUS) is a tool for assessing the usability of a variety of products and technologies such as the haptic feedback seat. Developed by Brooke [33], the questionnaire offers an efficient and technology-agnostic method for evaluating the usability and learnability of systems. The SUS consists of a 10-item questionnaire with five response options, ranging from "Strongly agree" to "Strongly disagree" as shown in Table III. The questionnaire is designed to be simple and straightforward, making it applicable to a wide range of user interfaces as well as comparative studies.

REFERENCES

[1] Transport Systems Catapult. *Market Forecast for Connected and Autonomous Vehicles*. (2017). Accessed: Jan. 26, 2024. [Online]. Available: https://assets.publishing.service.gov.uk/media/5a82466aed915d74e3402a89/15780_TSC_Market_Forecast_for_CAV_Report_FINAL.pdf

[2] I. Yaqoob, K. Hee, L.U. Khan, S.M. Ahsan Kazmi, M. Imran, N. Guizani, C.S. Hong "Autonomous Driving Cars in Smart Cities: Recent Advances, Requirements, and Challenges", IEEE Network, vol. 34, no. 1, pp. 174-181, 2020.

[3] SAE On-Road Automated Vehicle Standards Committee, "Taxonomy and definitions for terms related to on-road motor vehicle automated driving systems", SAE Standard Journal, vol. 3016, pp. 1-16, 2014.

[4] J.-L. Kaestle, B. Anvari, J. Krol, H.A. Wurdemann, "Correlation between Situational Awareness and EEG signals", Neurocomputing, vol. 432, pp. 70-79, 2021.

[5] N.A. Stanton, P.M. Salmon, G.H. Walker, E. Salas, P.A. Hancock, "State-of-science: Situation awareness in individuals, teams and systems", Ergonomics, vol. 60, no. 4, pp. 449-466, 2017.

[6] E. Yurtsever, J. Lambert, A. Carballo, K. Takeda, "A Survey of Autonomous Driving: Common Practices and Emerging Technologies", IEEE Access, vol. 8, pp. 58443-58469, 2020.

[7] H. Yun, J. Yang, "Multimodal warning design for take-over request in conditionally automated driving", European Transport Research Review, vol. 12, no. 34, pp. 1-11, 2020.

[8] W. Morales-Alvarez, O. Sipele, R. Leberon, H.H. Tadjine, C. Olaverri-Monreal, "Automated Driving: A Literature Review of the Take over Request in Conditional Automation", Electronics, vol. 9, no. 12, p. 2087, 2020.

[9] T. Nukarinen, J. Rantala, A. Farooq, R. Raisamo, "The effects of takeover request modalities on highly automated car control transitions", IEEE World Haptics Conference, pp. 345-350, 2015.

[10] S.H. Sol, Y.W. Kim, Y.G. Ji, "The effects of takeover request modalities on highly automated car control transitions", Accident Analysis & Prevention, vol. 123, pp. 150-158, 2019.

[11] J. Ryu, J. Chun, G. Park, S. Choi, S.H. Han, "Vibrotactile feedback for information delivery in the vehicle", IEEE Transactions on Haptics, vol. 3, no. 2, pp.138-149, 2010.

[12] Y. Zheng, J. Morrell, "Haptic actuator design parameters that influence affect and attention", IEEE Haptics Symposium, pp. 463-470, 2012.

[13] L. Lorenz, P. Kerschbaum, J. Schumann, "Designing take over scenarios for automated driving: How does augmented reality support the driver to get back into the loop?", Human Factors and Ergonomics Society Annual Meeting, vol. 58, no. 1, 2014.

[14] I. Politis, S Brewster, F. Pollick, "Language-based multimodal displays for the handover of control in autonomous cars", International Conference on Automotive User Interfaces and Interactive Vehicular Applications, pp. 3-10, 2015.

[15] S.M. Petermeijer, J.C. De Winter, K.J. Bengler, "Vibrotactile displays: A survey with a view on highly automated driving", IEEE Transactions on Intelligent Transportation Systems, vol. 17, no. 4, pp.897-907, 2015.

[16] S.M. Petermeijer, S. Cieler, J.C. De Winter, "Comparing spatially static and dynamic vibrotactile take-over requests in the driver seat", Accident Analysis & Prevention, vol. 99, pp. 218-227, 2017.

[17] W. Chang, W. Hwang, Y.G., "Haptic seat interfaces for driver information and warning systems", International Journal of Human-Computer Interaction, vol. 27, no. 12, pp. 1119-1132, 2011.

[18] A. Telpaz, B. Rhindress, I. Zelman, O. Tsimhoni, "Haptic seat for automated driving: preparing the driver to take control effectively", International Conference on Automotive User Interfaces and Interactive Vehicular Applications, pp. 23-30, 2015.

[19] G.M. Fitch, J.M. Hankey, B.M. Kleiner, T.A. Dingus, "Driver comprehension of multiple haptic seat alerts intended for use in an integrated collision avoidance system", Transportation Research Part F: Traffic Psychology and Behaviour, vol. 14, no. 4, pp. 278-290, 2011.

[20] Red Noland Cadillac. *Cadillac Active Safety - Safety Alert Seat*. (Aug. 28, 2017). Accessed: Jan.24, 2024.[Online Video]. Available: https://www.youtube.com/watch?v=X-CFFJbXE4A

[21] Lantal. *Pneumatic Comfort System - Aircraft - Lantal*. Accessed: Jan. 24, 2024. [Online]. Available: http://www.lantal.com/europe/en/aircraft/products/seat/pneumatic-comfort-system

[22] J.-P. Jeannet, T. Volery, H. Bergmann, C. Amstutz, "Company Profiles" Masterpieces of Swiss Entrepreneurship: Swiss SMEs Competing in Global Markets, pp. 299-561, 2021.

TABLE III
10-ITEM SUS QUESTIONNAIRE WITH FIVE RESPONSE OPTIONS [33].

		Strongly disagree				Strongly agree
1	I think that I would like to use this system frequently.	☐	☐	☐	☐	☐
2	I found the system unnecessarily complex.	☐	☐	☐	☐	☐
3	I thought the system was easy to use.	☐	☐	☐	☐	☐
4	I think that I would need the support of a technical person to be able to use this system.	☐	☐	☐	☐	☐
5	I found the various functions in this system were well integrated.	☐	☐	☐	☐	☐
6	I thought there was too much inconsistency in this system.	☐	☐	☐	☐	☐
7	I would imagine that most people would learn to use this system very quickly.	☐	☐	☐	☐	☐
8	I found the system very cumbersome to use.	☐	☐	☐	☐	☐
9	I felt very confident using the system.	☐	☐	☐	☐	☐
10	I needed to learn a lot of things before I could get going with this system.	☐	☐	☐	☐	☐

[23] Kongsberg Automotive. *Seat Support Systems: The Next Generation Comfort Seat*. Accessed: Jan. 24, 2024. [Online]. Available: http://mb.cision.com/Public/MigratedWpy/91591/712089/97869bf39eae352d.pdf

[24] R. Bhosale, N. Vogt, "Next generation of ventilated front seats", MSc dissertation, 2016.

[25] Continental. *Seat Comfort System*. Accessed: Jan. 26, 2024. [Online]. Available: https://www.continental-automotive.com/en/components/seat-comfort-system.html

[26] A.G. Barbu, M. Gheorghe, "Development of the car seat through a wider range of active elements implementation", Advanced Engineering Forum, vol 42, pp. 113-121, 2021.

[27] J. Peters, B. Anvari, C. Chen, Z. Lim, H. A. Wurdemann, "Hybrid fluidic actuation for a foam-based soft actuator", IEEE/RSJ International Conference on Intelligent Robots and Systems, pp. 8701-8708, 2020.

[28] P. Polygerinos, Z. Wang, J.T.B. Overvelde, K.C. Galloway, R.J. Wood, K. Bertoldi, C.J. Walsh, "Modeling of Soft Fiber-Reinforced Bending Actuators", IEEE Transactions on Robotics, vol. 31, no. 3, pp. 778-789, 2015.

[29] J.D. Van Der Laan, A. Heino, D. De Waard, "A simple procedure for the assessment of acceptance of advanced transport telematics", Transportation Research Part C: Emerging Technologies, vol. 5, no. 1, pp. 1-10, 1997.

[30] Y.G. Ji, K. Lee, W. Hwang, "Haptic perceptions in the vehicle seat", Human Factors and Ergonomics in Manufacturing & Service Industries, vol. 3, pp. 305–325, 2011.

[31] S.J. Lederman, R.L. Klatzky, "Haptic perception: a tutorial", Attention, Perception & Psychophysics, vol. 7, pp. 1439–1459, 2009.

[32] Festo. *Proportional-pressure regulator VPPM*. (2023). Accessed: Jan. 24, 2024. [Online]. Available: https://www.festo.com/media/pim/361/D15000100123361.PDF

[33] J. Brooke, "SUS: A quick and dirty usability scale", Usability Evaluation In Industry, vol. 189, 1995

[34] R.W. Ogden, "Non-Linear Elastic Deformations. Mineola", NY, USA: Courier Dover Publications, 1997.

[35] A.N. Gent, "A new constitutive relation for rubber", Rubber Chemistry and Technology, vol. 69, no. 1, pp. 59-61, 1996.

[36] C.O. Horgan, "The remarkable Gent constitutive model for hyperelastic materials", International Journal of Non-Linear Mechanics, vol. 68, pp. 9-16, 2015.

[37] S. Petermeijer, P. Hornberger, I. Ganotis, J. Winter, K. Bengler, "The Design of a Vibrotactile Seat for Conveying Take-Over Requests in Automated Driving", Advances In Human Aspects Of Transportation, pp. 618-630, 2018.

[38] B. Lewis, J. Eisert, C. Baldwin, "Effect of Tactile Location, Pulse Duration, and Interpulse Interval on Perceived Urgency", Transportation Research Record: Journal Of The Transportation Research Board, pp. 10-14, 2014.

[39] Y. Forster, S. Hergeth, F. Naujoks, J. Krems, A. Keinath, "Self-report measures for the assessment of human–machine interfaces in automated driving", Cognition, Technology & Work, vol. 22, pp. 703-720, 2020.

[40] Y. Zheng, E. Su, J.B. Morrell, "Design and evaluation of pactors for managing attention capture", World Haptics Conference, pp. 497–502, 2013.

[41] F. Roche, S. Brandenburg, "Should the Urgency of Visual-Tactile Takeover Requests Match the Criticality of Takeover Situations?", IEEE Transactions on Intelligent Vehicles, pp. 306-313, 2020.

[42] V. Rodday, B. Geißler, H. Ottersbach, M. Huelke, S. Letzel, A. Muttray, "Druckschmerzschwellen bei Druckreizen", GfA, Mainz, 2011.

[43] K. Reinmueller, A. Kiesel, M. Steinhauser, "Adverse Behavioral Adaptation to Adaptive Forward Collision Warning Systems: An Investigation of Primary and Secondary Task Performance", Accident, Analysis And Prevention, pp. 105718, 2020.

[44] A. Bangor, P. Kortum, J. Miller, "Determining What Individual SUS Scores Mean: Adding an Adjective Rating Scale", Journal Of Usability Studies, pp. 114-123, 2009.

[45] Y. Forster, F. Naujoks, A, Neukum, L. Huestegge, "Driver compliance to take-over requests with different auditory outputs in conditional automation", Accident, Analysis And Prevention, 109, pp. 18-28, 2017.

[46] X. Zhang, Y. Qiu, M.J. Griffin, "Developing a simplified finite element model of a car seat with occupant for predicting vibration transmissibility in the vertical direction", Ergonomics, vol. 58, no. 7, pp. 1220–1231, 2015.

[47] M. Bartholdt, M. Wiese, M. Schappler, S. Spindeldreier, A. Raatz, "A Parameter Identification Method for Static Cosserat Rod Models: Application to Soft Material Actuators with Exteroceptive Sensors", IEEE/RSJ International Conference on Intelligent Robots and Systems, pp. 624-631, 2021.

Jan Peters (Student Member, IEEE) received the B.S. degree in 2017 and the M.S. degree in 2020 from Leibniz University Hannover, Germany. Jan was working as a Research Fellow at UCL (UK) from 2019 to 2020 and was a visiting Researcher at Harvard University (USA) in 2022. He is currently working as a Research Assistant at the Institute of Assembly Technology (match) and pursuing a Ph.D degree at Leibniz University Hannover. His research interests include the design and evaluation of soft robotic systems and novel stiffening mechanisms.

Bani Anvari is Professor of Intelligent Mobility at UCL. She is the research leader of the Intelligent Mobility (IM) Group and Director of IM@UCL. She is interested in the complexity of interactions and how intuitive, intelligent, human-centric and personalised control systems can influence it. Her research focus has an emphasis on exploring driver and pedestrian interaction with semi- and fully-autonomous vehicles in different contexts (e.g., shared spaces, CAVs), an area of application that significantly benefits from robotics and AI.

Johann Licher is a mechanical engineering student at Leibniz University Hanover, Germany, and is working as a student research assistant at the Institute of Assembly Technology (match). He received the B.S. degree from Leibniz University of Hanover in 2022 and is currently a visiting student researcher at University College London, UK. Johann's research interests include biomedical devices and the development of soft robotic actuators.

Mats Wiese (Student Member, IEEE) received the B.S. degree from Technical University of Braunschweig, Germany, in 2015, and the M.S. degree from Leibniz University Hanover, Germany, in 2017. Mats is pursuing a PhD degree in Mechanical Engineering at Leibniz University Hanover since 2017 and is working as a Research Assistant at the Institute of Assembly Technology. His research focuses on modelling and control of soft pneumatic actuators in contact-rich environments.

Annika Raatz (Member, IEEE) is Professor of Mechanical Engineering at Leibniz University Hanover, Germany, and Head of the Institute of Assembly Technology (match) since 2013. After graduating (Dipl.-Ing.) in 1997, Annika received the Dr.-Ing. from Technical University of Braunschweig in 2006. Her primary areas of research are industrial robotic systems, task adapted synthesis of robot mechanisms, and the design of intelligent machine components for handling devices.

Helge A Wurdemann (Member, IEEE) is Professor of Robotics at University College London, leading robotics in the Department of Mechanical Engineering. He received a degree (Dipl.-Ing.) in electrical engineering with a focus on mechatronics and robotics in the medical field from the Leibniz University of Hanover, and a PhD in Robotics from King's College London in 2012. Helge has authored over 100 articles, published in high-impact journals, and peer-reviewed full-length conference papers.